Heat Transfer Across Metal-Dielectric Interfaces During Ultrafast-Laser Heating

Liang Guo

Stephen L. Hodson

Timothy S. Fisher

Xianfan Xu[1]

e-mail: xxu@purdue.edu

School of Mechanical Engineering
and Birck Nanotechnology Center,
Purdue University,
West Lafayette, IN 47907

Heat transfer across metal-dielectric interfaces involves transport of electrons and phonons accomplished either by coupling between phonons in metal and dielectric or by coupling between electrons in metal and phonons in dielectric. In this work, we investigate heat transfer across metal-dielectric interfaces during ultrafast-laser heating of thin metal films coated on dielectric substrates. By employing ultrafast-laser heating that creates strong thermal nonequilibrium between electrons and phonons in metal, it is possible to isolate the effect of the direct electron–phonon coupling across the interface and thus facilitate its study. Transient thermo-reflectance measurements using femtosecond laser pulses are performed on Au–Si samples while the simulation results based on a two-temperature model are compared with the measured data. A contact resistance between electrons in Au and phonons in Si represents the coupling strength of the direct electron–phonon interactions at the interface. Our results reveal that this contact resistance can be sufficiently small to indicate strong direct coupling between electrons in metal and phonons in dielectric. [DOI: 10.1115/1.4005255]

Keywords: interface thermal resistance, ultrafast laser, thermo-reflectance, two-temperature model, electron–phonon coupling

1 Introduction

Interface heat transfer is one of the major concerns in the design of microscale and nanoscale devices. In metal, electrons, and phonons are both energy carriers while in dielectric phonons are the main energy carrier. Therefore, for metal-dielectric composite structures, heat can transfer across the interface by coupling between phonons in metal and dielectric or by coupling between electrons in metal and phonons in dielectric through electron-interface scattering. Phonon–phonon coupling has been simulated mainly by the acoustic mismatch model and the diffuse mismatch model [1]. As for electron–phonon coupling, there are different viewpoints. Some studies have assumed that electron–phonon coupling across a metal-dielectric interface is negligible and heat transfer occurs as electron–phonon coupling within metal and then phonon–phonon coupling across the interface [2]. Electron–phonon coupling between metal (Cr, Ti, Al, Ni, and Pt) and SiO_2 has exhibited negligible apparent thermal resistance using a parallel-strip technique [3]. On the other hand, comparison between simulations and transient thermal reflectance (TTR) measurements for Au-dielectric interfaces reveals that energy could be lost to the substrate by electron-interface scattering during ultrafast-laser heating, and this effect depends on electron temperature and substrate thermal properties [4–6].

In this study, we employ TTR techniques to investigate interface heat transfer for thin gold films of varying thicknesses on silicon substrates. (Here, we consider silicon as a dielectric since heat is carried by phonons in silicon.) Similar work has been reported [5]. In our model, we consider two temperatures in metal and also the temperature in the dielectric substrate. This allows us to investigate the effect of both the coupling between electrons in metal and phonons in the dielectric substrate, and the coupling between phonons in metal and phonons in the dielectric substrate, and allows us to isolate the effect of the electron–phonon coupling across the interface that can be determined from the TTR measurement. Experimentally, we employ pulse stretching to minimize the effect of nonequilibrium among the electrons. As a result, the experimental data can be well-explained using the computational model. The thermal resistance between electrons in Au and phonons in Si, which quantifies the direct electron–phonon coupling strength, is calculated from the measured data. The results reveal that in the thermal nonequilibrium state, this electron–phonon coupling at the interface is strong enough to dominate the overall interface heat transfer.

2 TTR Measurement

Au–Si samples of varying Au thicknesses were prepared by thermal evaporation at a pressure of the order of 10^{-7} Torr. The thicknesses of the gold films are 39, 46, 60, 77, and 250 nm, measured using an atomic force microscope. The pump-and-probe technique is used in a collinear scheme to measure the thermo-reflectance signal. The laser pulses are generated by a Spectra Physics Ti:Sapphire amplified femtosecond system with a central wavelength of 800 nm and a repetition rate of 5 kHz. The wavelength of the pump beam is then converted to 400 nm with a second harmonic crystal. The pump pulse has a pulse width (full width at half maximum-FWHM) of 390 fs measured by the sum-frequency cross-correlation method and is focused onto the sample with a spot radius of 20.3 μm. The probe beam has a central wavelength of 800 nm and a pulse width of 205 fs measured by autocorrelation and is focused with a spot radius of 16.9 μm. This pump pulse width is intentionally stretched from the original pulse width of 50 fs to minimize the influence of thermal nonequilibrium among electrons since the electron thermalization time in Au can be of the order of 100 fs [7]. This thermalization time is pump wavelength and pump fluence dependent, and can be of the order of 10 fs if higher laser fluence is used [8,9]. Our experiments did show the importance of pulse stretching. Figure 1 shows the TTR measurement results for the sample of thickness 77 nm with different pump fluences before and after stretching the pulse. The plots show the normalized relative reflectance change $(-\Delta R/R)$

[1] Corresponding author.

Contributed by the Heat Transfer Division of ASME for publication in the JOURNAL OF HEAT TRANSFER. Manuscript received May 18, 2011; final manuscript received September 30, 2011; published online February 13, 2012. Assoc. Editor: Robert D. Tzou.

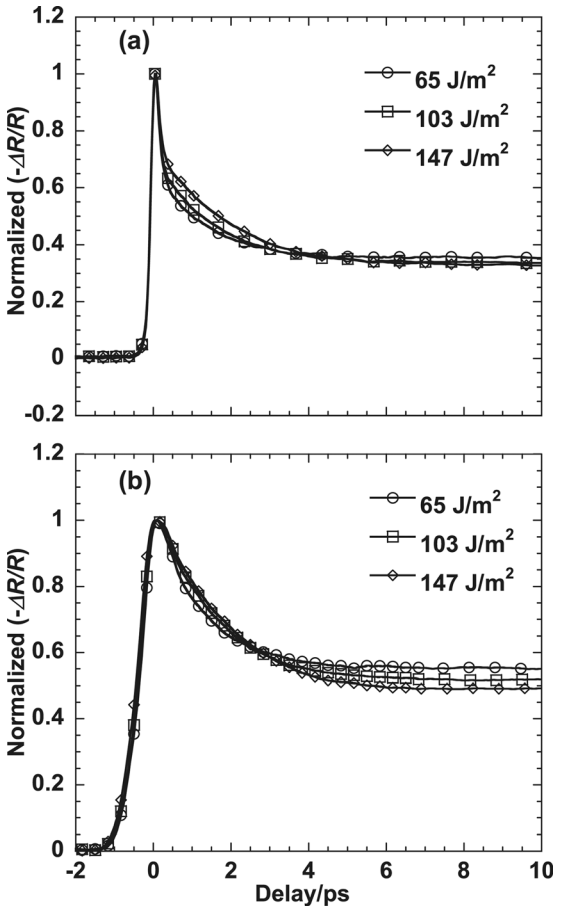

Fig. 1 TTR measurement results for the Au–Si sample of Au thickness 77 nm with different fluences. (*a*) Results before pulse stretching; (*b*) results after pulse stretching.

with the delay time between the pump and the probe pulses to show the contrast in cooling rates. With a shorter pulse (Fig. 1(*a*)), a steep initial drop is seen in the signal, which is attributed to the behavior of nonequilibrium among electrons. Since the TTM to be used for simulation assumes a well-defined temperature for electrons, i.e., the electrons in gold have reached thermal equilibrium (not necessarily a uniform temperature), the model cannot predict the fast initial drop in the signals in Fig. 1(*a*). As will be shown later, the signals obtained by stretching the pulse can be predicted well using the TTM.

3 Two-Temperature Model for Thermal Reflectance Measurements

Ultrafast-laser heating induces thermal nonequilibrium between electrons and phonons in metal, which can be described by the TTM [10–13]. We note that the heterogeneous interface considered here involves three primary temperature variables (two in the metal and one in the dielectric). The "two-temperature" model is applied to the metal side. For investigating electron–phonon and phonon–phonon coupling at the interface, two thermal resistances are defined: R_{es} (its reciprocal) indicates the coupling strength between electrons in metal and phonons in dielectric, while R_{ps} indicates the coupling strength between phonons in metal and phonons in dielectric. (Large thermal resistance corresponds to weak coupling.) The resulting governing equations, initial, and interface conditions are

$$C_e \frac{\partial T_e}{\partial t} = k_e \frac{\partial^2 T_e}{\partial x^2} - G(T_e - T_p) + S \tag{1a}$$

$$C_p \frac{\partial T_p}{\partial t} = k_p \frac{\partial^2 T_p}{\partial x^2} + G(T_e - T_p) \tag{1b}$$

$$C_s \frac{\partial T_s}{\partial t} = k_s \frac{\partial^2 T_s}{\partial x^2} \tag{1c}$$

$$T_e(t=0) = T_p(t=0) = T_s(t=0) = T_0 \tag{2}$$

$$-k_e \left.\frac{\partial T_e}{\partial x}\right|_{x=L} = \left.\frac{T_e - T_s}{R_{es}}\right|_{x=L} \tag{3a}$$

$$-k_p \left.\frac{\partial T_p}{\partial x}\right|_{x=L} = \left.\frac{T_p - T_s}{R_{ps}}\right|_{x=L} \tag{3b}$$

$$-k_s \left.\frac{\partial T_s}{\partial x}\right|_{x=L} = \left.\frac{T_e - T_s}{R_{es}}\right|_{x=L} + \left.\frac{T_p - T_s}{R_{ps}}\right|_{x=L} \tag{3c}$$

The subscripts e, p, and s denote electrons in metal, phonons in metal, and phonons in the dielectric substrate, respectively. C is the volumetric heat capacity, k is the thermal conductivity, G is the electron–phonon coupling factor governing the rate of energy transfer from electrons to phonons in metal, and L is the thickness of the metal layer. At the front surface of the metal layer insulation boundary condition is used due to the much larger heat flux caused by laser heating relative to the heat loss to air. At the rear surface of the substrate, since the thickness of the substrate used is large enough (1 μm) so that there is no temperature rise during the time period of consideration, the insulation boundary condition is also applied. Thermal properties of phonons in both metal and dielectric are taken as temperature-independent due to the weak temperature dependence. The thermal conductivity of phonons in metal is much smaller than that of the electrons and is taken in this work as 0.001 times the bulk thermal conductivity of gold (311 W/(mK)). The volumetric heat capacity of the metal phonon is taken as that of the bulk gold. C_e is taken as proportional to T_e [14] with the proportion coefficient being 70 J/(m^{3}K^2) [15], and k_e is calculated by the model and the data used in Ref. [13] which is valid from the room temperature to the Fermi temperature (6.39×10^4 K in Au, [14]). G can be obtained using the model derived in Ref. [16]. In this work, the value of G at the room temperature is taken as 4.6×10^{16} W/(m^{3}K) [17], and its dependence on electron and phonon temperatures follows [16]. The laser heating source term S is represented by the model used in [13] as

$$S = \frac{0.94(1-R)J}{t_p(\delta+\delta_b)\left[1-\exp\left(-\frac{L}{\delta+\delta_b}\right)\right]} \exp\left[-\frac{x}{\delta+\delta_b} - 2.77\left(\frac{t}{t_p}\right)^2\right] \tag{4}$$

which assumes all the absorbed laser energy is deposited in the metal layer. J is the fluence of the pump laser, R is the surface reflectance to the pump, t_p is the pulse width (FWHM), δ is the optical penetration depth, and δ_b is the electron ballistic length (around 100 nm in Au, [18]). R_{es} and R_{ps} are treated as free parameters for fitting the experimental data.

The wavelength of the probe laser in the experiment is centered at 800 nm. For this wavelength, the incident photon energy is below the interband transition threshold in Au, which is around 2.47 eV [18], and the Drude model can be used to relate the temperatures of electrons and phonons to the dielectric function and then the index of refraction, which is expressed as [19]

$$\varepsilon = \varepsilon_\infty - \frac{\omega_p^2}{\omega(\omega + i\omega_\tau)} \tag{5}$$

ω is the frequency of the probe laser and ω_p is the plasma frequency (1.37×10^{16} rad/s in Au evaluated using the data in Ref. [14]). ω_τ is the electron collisional frequency, the inverse of the electron relaxation time. The temperature dependence of electrical

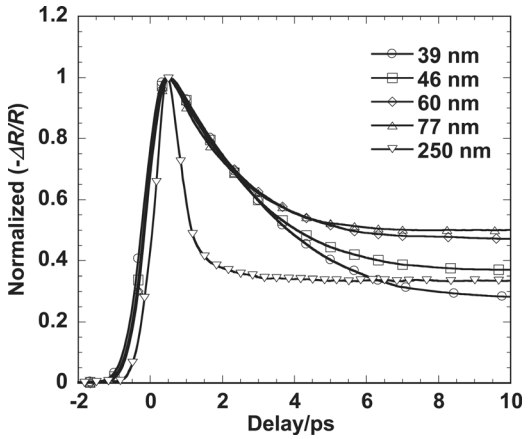

Fig. 2 TTR measurement results on Au–Si samples of varying Au thicknesses

resistivity indicates that ω_τ is approximately proportional to phonon temperature at high temperature [14] and from the Fermi liquid theory, its variation with electron temperature is quadratic (T_e^2) [20]. Therefore, ω_τ is related to T_e and T_p approximately as

$$\omega_\tau = A_{ee}T_e^2 + B_{ep}T_p \tag{6}$$

A_{ee} is estimated from the low-temperature measurement [21] and B_{ep} is usually estimated from the thermal or electrical resistivity near the room temperature [14]. In this work, A_{ee} is taken as the literature value 1.2×10^7 $s^{-1}K^{-2}$ [6] while ε_∞ and B_{ep} are evaluated by fitting the room-temperature value of the complex dielectric constant at 800 nm wavelength provided in Ref. [22], which are found to be 9.7 and 3.6×10^{11} $s^{-1}K^{-1}$, respectively. The complex index of refraction $n' + in''$ is the square root of the dielectric constant. Using Eqs. (5) and (6), n' and n'' are evaluated as 0.16 and 4.90, respectively, which agree with the empirical values [23]. The reflectance is then calculated from n' and n'' by the method of transfer matrix [24], which considers multiple reflections in thin films.

4 Results and Discussion

The results of TTR measurements with a pump fluence of 147 J/m^2 are plotted in Fig. 2. The fast decrease of the reflectance indicates that energy transfer between electrons and phonons in metal, followed by a relatively slow decrease after several ps which indicates electrons and phonons have reached thermal equilibrium. The initial cooling rates are smaller for samples with thicknesses less than the electron ballistic length since the electron temperature is almost uniform across the thin film, and coupling with phonons within the metal film and the dielectric substrate is the only cooling mechanism. For a thicker sample of thickness 250 nm, the initial decrease is much faster due to thermal diffusion in the gold film caused by a gradient of the electron temperature in the film.

We investigate the effect of R_{es} and R_{ps} using the thermoreflectance signal. Two values of R_{ps}, 1×10^{-10} m^{2}K/W and 1×10^{-7} m^{2}K/W, are used, each with a parameterized range of values for R_{es}. Figure 3 shows the calculated results for the sample with a 39 nm-thick gold film.

Little difference can be seen between Figs. 3(*a*) and 3(*b*) while different cooling rates are obtained with varying R_{es} in either plot, indicating that the cooling rate is not sensitive to the coupling strength between phonons in metal and dielectric. Note that an interface resistance of 1×10^{-10} m^{2}K/W is lower than any reported value, indicating a very high coupling strength between the phonons in metal and dielectric. Conversely, the results vary greatly with the coupling strength between electrons in metal and phonons in dielectric at the interface. This is because the lattice

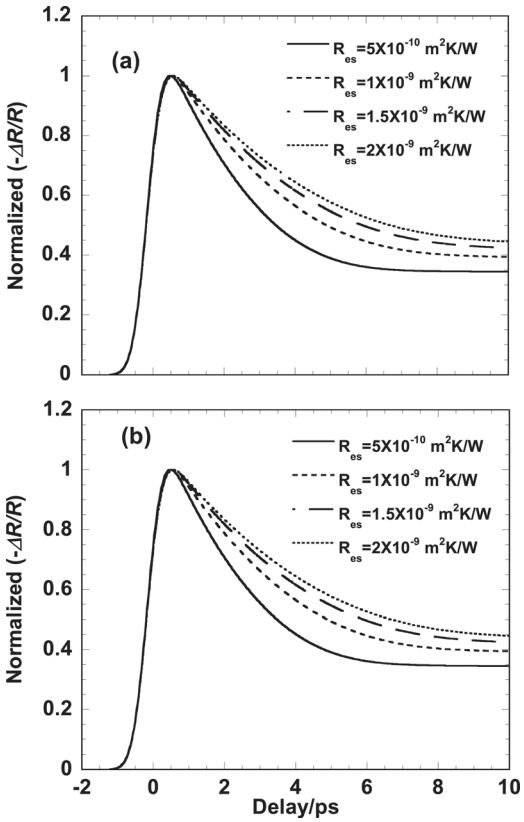

Fig. 3 Simulation results with varying R_{es} for the Au–Si sample of Au thickness 39 nm. (*a*) $R_{ps} = 1 \times 10^{-10}$ m^{2}K/W; (*b*) $R_{ps} = 1 \times 10^{-7}$ m^{2}K/W.

(phonon) temperature rise in metal is much smaller than the electron temperature that the interface coupling between phonons in metal and dielectric does not influence the surface temperature, which directly determines the measured reflectance. On the other hand, the temperature rise of electrons is much higher, and consequently, the cooling rate is sensitive to R_{es}. The relatively high sensitivity of R_{es} to that of R_{ps} demonstrates that the former can be isolated for the study of the coupling between electrons in metal and phonons in dielectric.

We now use the measured TTR data to estimate R_{es}, the thermal resistance between electrons in metal and phonons in dielectric. R_{es} is adjusted by the least square method to fit the simulation results with the measured data, and the results are shown in Fig. 4. We note that it is impossible to fit the measured results using insulation interface condition (i.e., no coupling or extremely large thermal resistance between electrons in metal and phonons in the dielectric substrate), which will significantly underestimate the cooling rate. For thin samples, we find that the value of R_{es} is of the order of 10^{-10} to 10^{-9} m^{2}K/W. This value is below the thermal resistances of representative solid–solid interfaces measured in thermal equilibrium [25]. This indicates that the direct coupling between electrons in metal and phonons in dielectric is strong. It is also noted that the resistance values increases with the thickness of the gold film, indicating a decrease in the coupling strength between electrons in metal and the dielectric substrate. This could be due to the lower electron temperature obtained in thicker films, and a decrease of the coupling strength with a decrease in the electron temperature [5]. For the sample of thickness 250 nm, R_{es} has little effect on the simulation result since the interface is too far from the absorbing surface to influence the surface temperature, and therefore it is not presented here.

The agreement between the fitted results and the measured data is generally good. The small discrepancy between the measured and the fitted results can result from inaccuracy in computing the

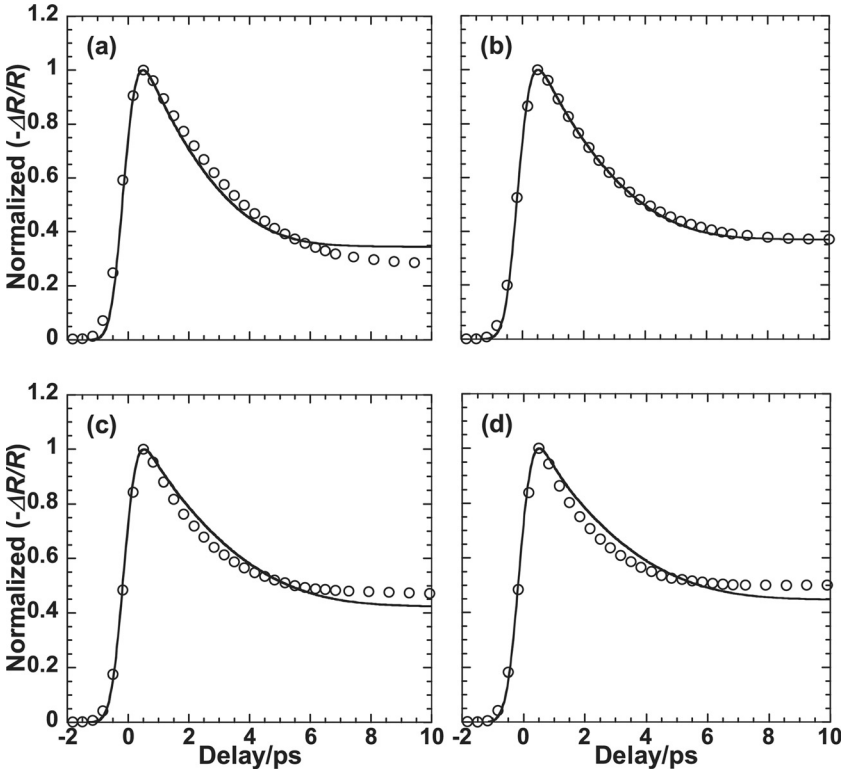

Fig. 4 Comparison between the measurement and the simulation results for Au–Si samples of different Au thicknesses. The open circle represents the measured data and the solid line represents the simulation results. (*a*) 39 nm fitted by $R_{es} = 5 \times 10^{-10}$ m^{2}K/W; (*b*) 46 nm fitted by $R_{es} = 6 \times 10^{-10}$ m^{2}K/W; (*c*) 60 nm fitted by $R_{es} = 1.2 \times 10^{-9}$ m^{2}K/W; and (*d*) 77 nm fitted by $R_{es} = 1.8 \times 10^{-9}$ m^{2}K/W.

absorption or the temperature. Figure 1(b) shows the normalized TTR measurement results on the sample of thickness 77 nm with three laser fluences. It is seen that small variations in the shape of the TTR signals can be caused by different laser fluences and thus the maximum temperature reached in the film. Absorption in metal, multiple reflections between the metal surface and the Au–Si interface, and possible deviations of the properties of thin films from those of bulk can all contribute to uncertainties in the temperature simulation; therefore affecting the calculated reflectance.

With the values of R_{es} shown in Fig. 4, the calculation shows that the highest electron temperature, which is at the surface of 39 nm–thick gold film, is about 6700 K. The highest temperature of electrons is roughly inversely proportional to the thickness of the films for the four thinner films. The highest temperature of electrons is much less than the Fermi temperature and thus ensures the validity of the linear dependence of C_e on T_e [14]. The highest temperature for the lattice in metal is about 780 K, also in the 39 nm-thick gold film. This large temperature difference between electrons and lattice indicates that the interface heat transfer is dominated by the coupling between electrons in metal and the phonons in the dielectric substrate. As shown in Fig. 4, the measured R_{es} is very low, of the order of 10^{-10} to 10^{-9} m^{2}K/W. Even if R_{ps}, which is not determined in this study, is also that low (note that 10^{-10} to 10^{-9} m^{2}K/W is lower than any reported values), because of the large difference in temperatures between electrons and the phonons in metal, the interface heat transfer rate (Eqs. (3*a*)–(3*c*)) due to the coupling between electrons in metal and the substrate is much larger than that due to the coupling between phonons in metal and the substrate.

5 Conclusions

In conclusion, TTR measurements using femtosecond laser pulses are performed on Au–Si samples and the results are analyzed using the TTM model. It is shown that due to the strong nonequilibrium between electrons and phonons during ultrafast-laser heating, it is possible to isolate the effect of the direct electron–phonon coupling across the interface, allowing investigation of its strength. Using stretched femtosecond pulses is shown to be able to minimize the nonequilibrium effect among electrons, and is thus more suitable for this study. The TTR measurement data can be well-represented using the TTM model. Comparison between the TTR data and the TTM results indicates that the direct coupling due to electron-interface scattering dominates the interface heat transfer during ultrafast-laser heating of thin films.

Acknowledgment

This paper is based upon work supported by the Defense Advanced Research Projects Agency and SPAWAR Systems Center, Pacific under Contract No. N66001-09-C-2013. The authors also thank C. Liebig, Y. Wang, and W. Wu for helpful discussions.

Nomenclature

A_{ee} = coefficient in Eq. (6), s^{-1}K^{-2}
B_{ep} = coefficient in Eq. (6), s^{-1}K^{-1}
C = volumetric heat capacity, J/(m^{3}K)
G = electron–phonon coupling factor, W/(m^{3}K)
i = unit of the imaginary number
J = fluence of the pump, J/m^2
k = thermal conductivity, W/(mK)
L = metal film thickness, m
n' = real part of the complex index of refraction
n'' = imaginary part of the complex index of refraction
R = interface thermal resistance, m^{2}K/W; reflectance
S = laser source term, W/m^3

T = temperature, K
t = time, s
t_p = pulse width of the pump (FWHM), s
x = spatial coordinate, m
ε = complex dielectric constant
ε_∞ = constant in the Drude model
δ = radiation penetration depth, m
δ_b = electron ballistic depth, m
ω = angular frequency of the probe, rad/s
ω_p = plasma frequency, rad/s
ω_τ = electron collisional frequency, rad/s

Subscripts

0 = initial state
e = electron in metal
es = electron in metal and phonon in dielectric
p = phonon in metal
ps = phonon in metal and phonon in dielectric
s = phonon in dielectric

References

[1] Cahill, D. G., Ford, W. K., Goodson, K. E., Mahan, G. D., Majumdar, A., Maris, H. J., Merlin, R., and Phillpot, S. R., 2003, "Nanoscale Thermal Transport," J. Appl. Phys., **93**(2), pp. 793–818.

[2] Majumdar, A., and Reddy, P., 2004, "Role of Electron–Phonon Coupling in Thermal Conductance of Metal–Nonmetal Interfaces," Appl. Phys. Lett., **84**(23), pp. 4768–4770.

[3] Chien, H.-C., Yao, D.-J., and Hsu, C.-T., 2008, "Measurement and Evaluation of the Interfacial Thermal Resistance Between a Metal and a Dielectric," Appl. Phys. Lett., **93**(23), p. 231910.

[4] Hopkins, P. E., and Norris, P. M., 2007, "Substrate Influence in Electron–Phonon Coupling Measurements in Thin Au Films," Appl. Surf. Sci., **253**(15), pp. 6289–6294.

[5] Hopkins, P. E., Kassebaum, J. L., and Norris, P. M., 2009, "Effects of Electron Scattering at Metal–Nonmetal Interfaces on Electron-Phonon Equilibration in Gold Films," J. Appl. Phys., **105**(2), p. 023710.

[6] Hopkins, P. E., 2010, "Influence of Electron-Boundary Scattering on Thermoreflectance Calculations After Intraband and Interband Transitions Induced by Short-Pulsed Laser Absorption," Phys. Rev. B, **81**(3), p. 035413.

[7] Sun, C.-K., Vallee, F., Acioli, L., Ippen, E. P., and Fujimoto, J. G., 1993, "Femtosecond Investigation of Electron Thermalization in Gold," Phys. Rev. B, **48**(16), pp. 12365–12368.

[8] Fann, W. S., Storz, R., Tom, H. W. K., and Bokor, J., 1992, "Electron Thermalization of Gold," Phys. Rev. B, **46**(20), pp. 13592–13595.

[9] Fann, W. S., Storz, R., Tom, H. W. K., and Bokor, J., 1992, "Direct Measurement of Nonequilibrium Electron-Energy Distributions in Subpicosecond Laser-Heated Gold Films," Phys. Rev. Lett., **68**(18), pp. 2834–2837.

[10] Kaganov, M. I., Lifshitz, I. M., and Tanatarov, L. V., 1957, "Relaxation Between Electrons and the Crystalline Lattice," Sov. Phys. JETP, **4**(2), pp. 173–178.

[11] Anisimov. S. I., Kapeliovich, B. L., and Perel'man, T. L., 1974, "Electron Emission From Metal Surfaces Exposed to Ultrashort Laser Pulses," Sov. Phys. JETP, **39**(2), pp. 375–377.

[12] Qiu, T. Q., and Tien, C. L., 1993, "Heat Transfer Mechanisms During Short-Pulse Laser Heating of Metals," ASME Trans. J. Heat Transfer, **115**(4), pp. 835–841.

[13] Chowdhury, I. H., and Xu, X., 2003, "Heat Transfer in Femtosecond Laser Processing of Metal," Numer. Heat Transfer, Part A, **44**(3), pp. 219–232.

[14] Kittel, C., 1976, *Introduction to Solid State Physics*, John Wiley & Sons, Inc., New York.

[15] Smith, A. N., and Norris, P. M., 2001, "Influence of Intraband Transitions on the Electron Thermoreflectance Response of Metals," Appl. Phys. Lett., **78**(9), pp. 1240–1242.

[16] Chen, J. K., Latham, W. P., and Beraun, J. E., 2005, "The Role of Electron–Phonon Coupling in Ultrafast Laser Heating," J. Laser Appl., **17**(1), pp. 63–68.

[17] Hostetler, J. L., Smith, A. N., Czajkowsky, D. M., and Norris, P. M., 1999, "Measurement of the Electron-Phonon Coupling Factor Dependence on Film Thickness and Grain Size in Au, Cr, and Al," Applied Optics, **38**(16), pp. 3614–3620.

[18] Hohlfeld, J., Wellershoff, S.-S., Gudde, J., Conrad, U., Jahnke, V., and Matthias, E., 2000, "Electron and Lattice Dynamics Following Optical Excitation of Metals," Chem. Phys., **251**(1–3), pp. 237–258.

[19] Maier, S. A., 2007, *Plasmonics: Fundamentals and Applications*, Springer Science + Business Media, New York.

[20] Ashcroft, N. W., and Mermin, N. D., (1976), *Solid State Physics*, W. B. Saunders, Philadelphia.

[21] MacDonald, A. H., 1980, "Electron-Phonon Enhancement of Electron-Electron Scattering in Al," Phys. Rev. Lett., **44**(7), pp. 489–493.

[22] Johnson, P. B., and Christy, R. W., 1972, "Optical Constants of the Noble Metals," Phys. Rev. B, **6**(12), pp. 4370–4379.

[23] Palik, E. D., (1998), *Handbook of Optical Constants of Solids*, Academic, San Diego.

[24] Pedrotti, F. L., Pedrotti, L. S., and Pedrotti, L. M., (2007), *Introduction to Optics*, Pearson Prentice Hall, Upper Saddle River, NJ.

[25] Incropera, F. P., Dewitt, D. P., Bergman, T. L., and Lavine, A. S., 2007, *Fundamentals of Heat and Mass Transfer*, John Wiley & Sons, Inc., Hoboken, NJ.